Available online at www.sciencedirect.com
SCIENCE DIRECT®
Comput. Methods Appl. Mech. Engrg. 193 (2004) 5129–5141
Computer methods in applied mechanics and engineering
www.elsevier.com/locate/cma

Coarse-grained models of materials with non-convex free-energy: two case studies

Antonio DeSimone

SISSA, International School for Advanced Studies, Via Beirut 2-4, 340014 Trieste, Italy

Received 17 May 2003; received in revised form 18 December 2003; accepted 18 December 2003

Abstract

Bridging across length scales is one of the fundamental challenges in the computational modelling of material systems whose mechanical response is driven by rough energy landscapes. The typical feature of such systems is that of exhibiting fine scale microstructures. Two case studies, namely, nematic elastomers and ferromagnetic shape memory alloys, are presented to illustrate the use of modern techniques from (non-convex) calculus of variations in developing coarse-grained models of microstructure-driven material response.

PACS: 61.41.+e; 75.80.+q; 46.15.−x
Keywords: Microstructures; Phase transformations; Quasi-convexity; Shape memory alloys; Ferromagnetism; Nematic liquid crystals; Elastomers

1. Introduction

This paper is concerned with the mechanical implications of pattern formation driven by rough energy landscapes and with the computational modelling of the macroscopic response of materials exhibiting (reversible, displacive) phase transformations upon loading.

The conceptual framework in which our discussion takes place is the following. Equilibrium domain patterns often emerge in physical systems whose free-energy density is non-convex. We call such an energy density a multiwell potential. In these circumstances, configurations in which the state variables only take values in the minima of the potential (i.e., they lie on the material's energy wells) are energetically favored. If boundary conditions (or more subtle effects, such as non-local dipolar interactions in the case of systems

E-mail address: desimone@sissa.it

0045-7825/$ - see front matter
doi:10.1016/j.cma.2003.12.064

exhibiting strong mechanical electro-magnetic coupling) do not allow the system to assume a spatially uniform configuration resting entirely on a single energy well, then domain structures emerge. Through the application of external loads (forces, electro-magnetic fields, changes in imposed boundary conditions) one may alter the energy balance among the wells, so that some are favored. This results in domain switching, i.e., a rearrangement of domain structures which leads to soft deformation paths (accompanied by a plateau in the stress–strain response in purely mechanical systems, or by enhanced deformations at relatively small electro-magnetic fields in electrostrictive or magnetostrictive materials) that are of great technological relevance.

A typical exemplification of the type of processes just described is super-elasticity in shape memory alloys. Numerous contributions to the modelling of this phenomenon have already come from the Computational Plasticity community, typically exploiting phenomenological approaches based on the use of internal variables (see, e.g., [24]). The point of view we wish to emphasize here is, however, different and more micromechanical in spirit. We are interested in attempts at confronting openly the complex multiscale nature of the response of systems described by multiwell potentials. In particular, we are interested in the microscopic origin of the observed macroscopic response and in the development of computational strategies which on one hand are directly based on the microscopic mechanisms of evolution of domain structures and, on the other hand, provide explicit information on the essentials of microstructure evolution underpinning the macroscopic behavior.

Needless to say, the challenge is quite formidable. There is, however, progress to be reported not only in the development of a general conceptual framework (see, e.g., [1,25]), but also in its application to concrete material systems. This paper reviews two recent case studies in which the author was involved that can be used to support this claim. They both address quasi-static response, and they are both based on global energy minimization. The first one (nematic elastomers) concerns a purely mechanical system which is studied from the point of view of non-linear elasticity, employing finite deformation kinematics. The second one (ferromagnetic shape memory alloys) addresses the issue of coupling mechanics and electro-magnetism, and it is based on linearized kinematics (i.e., small deformations). Both examples make decisive use of material symmetry in circumventing some of the technical problems that often hinder the explicit derivation of macroscopic constitutive laws from the underlying microstructural mechanisms.

The modest successes reported in what follows should in no way mislead the reader in underestimating the efforts that are needed to further advance the program of bridging across length scales in computational mechanics. Even for materials which are well described by multiwell potentials, extensions to more anisotropic solids (for which material symmetry yields less spectacular simplifications), modelling of hysteresis and of dissipation mechanisms, evaluation of the macroscopic impact of the kinetics of microstructural evolution are truly necessary steps. We do hope, however, that a moderately optimistic assessment of some recent progress will provide enough motivation for others to join these efforts.

2. Nematic elastomers

Nematic elastomers consist of networks of cross-linked polymeric chains, each of which contains nematic rigid rod-like molecules [21]. These are called nematic mesogens: their tendency to align below a critical transition temperature promotes the formation of nematic order. Contrary to nematic liquids, however, the orientational degrees of freedom of the mesogens are coupled to the translational degrees of freedom of an underlying elastic solid (the rubbery polymer network). This coupling makes nematic elastomers very interesting as a model physical system, and it is also at the root of their technological interest as (mechanically tunable) optical wave-guides. Other speculative applications of nematic elastomers, linked exclusively to the mechanical material instabilities to be discussed below, are in the field of artificial muscles.

Nematic elastomers display interesting material instabilities [34]. At high temperatures, the nematic mesogens are randomly oriented due to thermal fluctuations, and nematic elastomers behave-like isotropic rubbers. Upon cooling through the nematic transition temperature, nematic mesogens align and the rubber network deforms uniaxially, as dictated by symmetry, with distinguished axis parallel to the common direction of the mesogens. Different directions of the optical axis, hence different states of spontaneous distorsion may coexist in a sample, giving rise to domain patterns observable under polarized light (regions where the mesogens are differently oriented may appear opaque or transparent when observed under crossed polarizers, depending of the relative orientation of mesogens and polarization of light). Moreover, the existence of domain patterns allows nematic elastomers to respond to imposed macroscopic deformations with negligible internal stress, whenever the imposed strains may be accommodated by simply reorienting the nematic mesogens.

Both the occurrence of domains, in a characteristic striped texture, and the existence of 'soft' deformation modes have been observed experimentally [22]. An expression for the system's free-energy has been proposed, and it has been shown how the observed phenomena can be interpreted as attempts of the system to minimize the proposed (non-convex) free-energy [2].

Our interest in nematic elastomers arose from the realization that at the root of their fascinating material instabilities (domain formation and soft deformation paths) there is a symmetry breaking phase transformation (from the high temperature isotropic phase to the low temperature nematic phase), in close analogy with martensitic phase transformations. While in the latter case, however, the underlying material symmetry is the discrete crystallographic symmetry of the parent phase, in the case of nematic elastomers the full isotropic symmetry of the high temperature amorphous polymer is available. It soon became apparent that the mathematical techniques developed for the study of displacive phase transformations in crystals are applicable to a radically different class of systems (polymers, rather than crystals) and that the simplifications accompanying the enhanced material symmetries lead to results of unprecedented completeness.

Based on the intuitive background outlined above, the free-energy formula proposed in [2], which uses as reference configuration one of the observable stress-free configurations of the nematic product phase, has been rewritten in [12] by performing an affine change of variables leading to the use of a new reference configuration, namely, the highly symmetric stress-free configuration of the isotropic parent phase. The resulting expression, after minimization over the nematic degrees of freedom (described by a unit vector field $\mathbf{n}$, called director), reads

$$W(\mathbf{F}) = \begin{cases} \lambda_1^2(\mathbf{F}) + \lambda_2^2(\mathbf{F}) + a\lambda_3^2(\mathbf{F}) - 3a^{1/3} & \text{if } \det \mathbf{F} = 1, \\ +\infty & \text{else}, \end{cases} \tag{1}$$

where $\lambda_1(\mathbf{F}) \leqslant \lambda_2(\mathbf{F}) \leqslant \lambda_3(\mathbf{F})$ are the ordered principal stretches associated with the deformation gradient $\mathbf{F} = \nabla \mathbf{y}$, $\mathbf{y}$ being the deformation. The scalar $a < 1$ is a material parameter related to the distorsion that the polymeric chains suffer with the establishment of nematic order. A further material parameter, which would appear in (1) as a global multiplicative constant, and which measures the shear modulus in the natural configuration, has been normalized to one. Notice also that incompressibility has been assumed, leading to the constraint $\det \mathbf{F} = 1$ on deformations with finite energy. It is also interesting to remark that, for $a = 1$, (1) reduces to the classical neohookean expression. Finally, it should be noted that, as a byproduct of the minimization over the nematic degrees of freedom leading to (1), it is known that the director $\mathbf{n}$ is always aligned with the eigenvector of $\mathbf{F}\mathbf{F}^{\mathrm{T}}$ associated with its largest eigenvalue $\lambda_3^2(\mathbf{F})$.

Energy (1) is non-convex. This implies that uniform configurations may have higher energies than complex microscopic domain patterns with the same average deformation. As noted above, this fact is at the root of the proposed explanations for the experimental observations showing that uniformly deformed samples of nematic elastomers may spontaneously break up into domains, by developing a characteristic striped texture. The non-convexity of (1) also explains the experimentally observed soft deformation paths.

These arise as energetically optimal fine phase mixtures, with volume fractions evolving with the applied loads, which effectively accomplish a convexification of the underlying rough energy landscape. A plateau in the stress–strain response is, in fact, the signature of a flat portion of the energy graph resulting from a suitable convexification of the energy. Macroscopic soft deformation paths can thus be fully characterized as suitable convex hulls of the material's energy wells, see [13].

Moving now to the issue of resolving numerically the details of a realistic boundary value problem, complex enough to be able to help in understanding the outcome of actual laboratory experiments, the multiscale nature of the problem at hand poses a drastic alternative. On one hand, one may try and resolve the fine details of the microstructures, and obtain the relevant macroscopic information by averaging. Energy (1) does not contain an intrinsic length scale. Its minimization can lead to microstructures with no characteristic length, which manifest themselves as infinitely refining minimizing sequences of deformation patterns. In order to resolve length scales, models containing higher order gradients (e.g., Frank-type terms) need to be considered, see e.g., [18,19], with very severe consequences in terms of computational costs.

Alternatively, one may insist on a direct macroscopic approach, in which only the essentials of the underlying microscopic processes are explicitly resolved. In this case, the key observation is that the expression (1) does not represent correctly the energetic cost of imposing the affine deformation $\mathbf{F}$ on a representative volume element. This is instead given by the so-called quasi-convex envelope of W [25],

$$W_{\mathrm{qc}}(\mathbf{F}) = \inf_{\mathbf{y}\in W^{1,\infty}} \left\{ \frac{1}{|\Omega|} \int_{\Omega} W(\nabla \mathbf{y}(\mathbf{x}))\mathrm{d}\mathbf{x} : \mathbf{y}(\mathbf{x}) = \mathbf{F}\mathbf{x} \text{ on } \partial\Omega, \det \nabla \mathbf{y}(\mathbf{x}) = 1 \right\}, \tag{2}$$

which coarse-grains the energetics of the system. Indeed, $W_{\mathrm{qc}}(\mathbf{F})$ gives the minimum energy needed to deform the region Ω according to the macroscopic deformation $\mathbf{F}$, optimized over all possible admissible microstructures $\mathbf{y}(\mathbf{x})$ with average gradient $\mathbf{F}$. Here the notation $\mathbf{y} \in W^{1,\infty}$ means that $\mathbf{y}$ is Lipschitz-continuous. We emphasize that the domain Ω appearing in (2), whose volume we denote by $|\Omega|$, plays here the role of a representative volume element: it can be verified that W_{qc} does not depend on the geometry of Ω. The use of W_{qc} in the numerical computations allows one to resolve only the macroscopic length scale, with the (possibly infinitesimal) microscopic scale already accounted for in W_{qc}.

For nematic elastomers, an explicit formula for W_{qc} has been derived in [14], which for volume-preserving deformation gradients reads

$$W_{\mathrm{qc}}(\mathbf{F}) = \begin{cases} 0 & \text{if } \lambda_1 \geqslant a^{1/6} \quad \text{(phase L)}, \\ W(\mathbf{F}) & \text{if } a^{1/2}\lambda_3^2\lambda_1 > 1 \quad \text{(phase S)}, \\ \lambda_1^2 + 2a^{1/2}\lambda_1^{-1} - 3a^{1/3} & \text{else} \quad \text{(phase Sm)} \end{cases} \tag{3}$$

while it is infinite if $\det \mathbf{F} \neq 1$.

The three regimes in (3) arise from the collective behavior of energetically optimal fine phase mixtures. They represent three different modes of macroscopic mechanical response corresponding to three different patterns of decomposition of the average deformation gradient $\mathbf{F}$. Phase L describes a liquid-like response (at least within the ideally soft approximation embedded in the expression (1) for the microscopic energy density), and it is typically accompanied by relatively complex microstructures (layers-within-layers). Phase S shows no fine phase mixtures, and the coarse-grained energy reproduces the microscopic one with no changes. Finally the smectic-like phase Sm exhibits simple (i.e., simple layers) microstructures which, in contrast with the L phase, have the capability of transmitting internal stresses.

Besides shedding light on the microstructural origin of the observable macroscopic response, the phase diagrams locating a given macroscopic deformations within one of the three phases L, S, Sm are also useful in reconstructing, from the field of computed local deformation gradients $x \mapsto \mathbf{F}(x)$, the corresponding field of local (energy minimizing) microstructures, see Fig. 1.

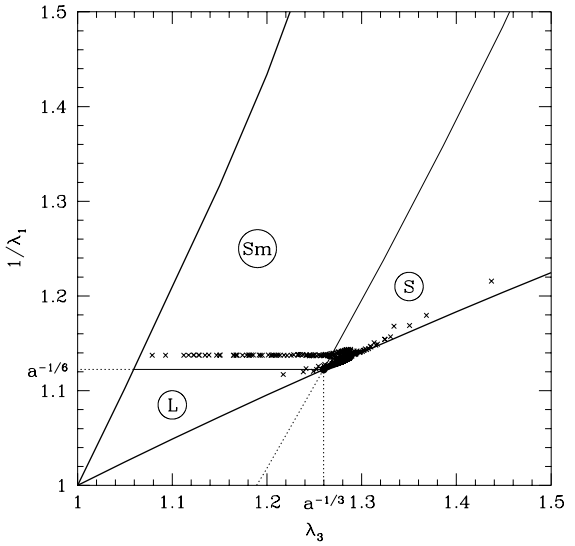

Fig. 1. Phase diagram for nematic elastomers corresponding to Eq. (2) with $a = 1/2$. Here the crosses give the location of the computed deformation gradients corresponding to $s = 1.38$ in Fig. 5 (adapted from [7]).

To gain an understanding of the structure of the energy density (and of the technical difficulties involved in proving the formula), consider the case of a macroscopic deformation gradient described by

$$\mathbf{F}_t = \begin{pmatrix} a^{1/6} & 0 & 0 \\ 0 & \lambda(t) & 0 \\ 0 & 0 & a^{-1/6}/\lambda(t) \end{pmatrix}, \tag{4}$$

where $\lambda(t)$ increases from $\lambda(0) = a^{1/6}$ to $\lambda(1) = a^{-1/3}$ as the loading parameter t increases from zero to one. It easy to show (by using the classical inequality between arithmetic and geometric mean) that, under the condition $\det \mathbf{F} = \lambda_1^2(\mathbf{F})\lambda_2^2(\mathbf{F})\lambda_3^2(\mathbf{F}) = 1$, the energy density (1) is non-negative, and it vanishes only if $\lambda_1(\mathbf{F}) = \lambda_2(\mathbf{F}) = a^{1/6}$ and $\lambda_3(\mathbf{F}) = a^{-1/3}$. Thus, for $0 < t < 1$, i.e., for all values $\lambda(t) \in]a^{1/6}, a^{-1/3}[$, one has $W(\mathbf{F}_t) > 0$. This means that a sample which is homogeneously deformed according to (4) stores positive energy. However, the (macroscopic) deformation $\mathbf{F}_t$ can be accommodated at zero energy by forming a fine microstructure mixing the two (microscopic) deformation gradients

$$\mathbf{F}_t^{\pm} = \begin{pmatrix} a^{1/6} & 0 & 0 \\ 0 & \lambda(t) & \pm\delta(t) \\ 0 & 0 & a^{-1/6}/\lambda(t) \end{pmatrix}. \tag{5}$$

Indeed, for $\delta^2 = (a^{-2/3} - \lambda^2)(1 - a^{1/3}\lambda^{-2})$, one has $W(\mathbf{F}_t^{\pm}) = 0$. Moreover, since Hadamard's kinematic compatibility condition

$$\mathbf{F}_t^{+} - \mathbf{F}_t^{-} = \mathbf{a} \otimes \mathbf{n} \tag{6}$$

is satisfied with $\mathbf{n} = \mathbf{e}_3$ and $\mathbf{a} = 2\delta(t)\mathbf{e}_2$, there exists a continuous deformation $\mathbf{y}_t$, whose gradient takes only the two values $\mathbf{F}_t^{\pm}$, alternating them in layers orthogonal to $\mathbf{n}$. If the layers are of equal width, as their size becomes increasingly finer, then the deformation $\mathbf{y}_t$ converges uniformly to the affine deformation with gradient $\mathbf{F}_t = (\mathbf{F}_t^{+} + \mathbf{F}_t^{-})/2$ (see Fig. 2 for a sketch). The argument just outlined gives, in fact, a simple energetic interpretation of the stripe domain patterns observed experimentally in [22], see also [33].

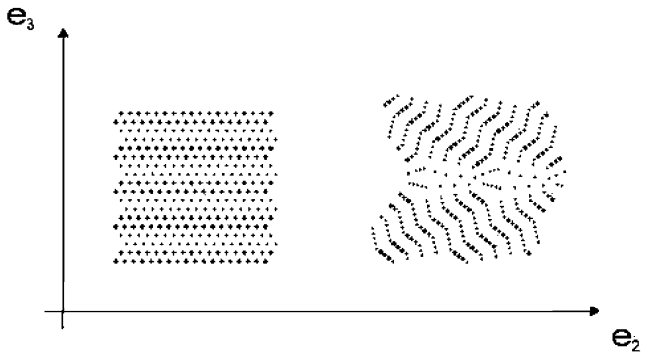

Fig. 2. A sketch of typical microstructures: simple layers (left panel), see Eq. (5), and layers within layers (right panel). The light and dark dots hints at the optical contrast these microstructure would produce in nematic elastomers under polarized light (adapted from [12]).

Moving to more complex states of deformation, we observe that the liquid-like response of phase L is associated with formation of microstructure and no internal stress. For this to occur, it is required that, simultaneously, $\lambda_1(\mathbf{F}) \geqslant a^{1/6}$ and $\lambda_3(\mathbf{F}) \leqslant a^{-1/3}$. If $\lambda_1(\mathbf{F}) = a^{1/6}$, then the underlying microstructures are the simple layers associated with (5). If $\lambda_1(\mathbf{F}) > a^{1/6}$ (in particular, if $\lambda_1(\mathbf{F}) = \lambda_3(\mathbf{F})$, i.e., if $\mathbf{F}$ is the identity), then a more complex microstructure is needed (layers within layers, see Fig. 2 for a sketch). The solid-like response of phase S is characterized by stress transmission with no microstructure formation. It occurs if the largest principal stretch $\lambda_{\max} := \lambda_3(\mathbf{F})$ of the imposed deformation $\mathbf{F}$ is large enough, i.e., if

$$\lambda_{\max} > \Lambda^*(\lambda_{\min}) := (a^{1/2}\lambda_{\min})^{-\frac{1}{2}}, \quad \lambda_{\min} \leqslant a^{1/6}. \tag{7}$$

Note that if $\lambda_{\min} := \lambda_1(\mathbf{F}) = a_{1/6}$, then $\Lambda^* = a^{-1/3}$. Finally, the smectic-like response of phase Sm entails formation of microstructure at non-zero internal stress, and it arises if the smallest principal stretch $\lambda_{\min} = \lambda_1(\mathbf{F})$ is small enough

$$\lambda_{\min} < \Lambda_*(\lambda_{\max}) := \begin{cases} (a^{1/2}\lambda_{\max}^2)^{-1} & \text{if } \lambda_{\max} \geqslant a^{-1/3}, \\ a^{1/6} & \text{else.} \end{cases} \tag{8}$$

The underlying microstructures are simple layers. This discussion is summarized schematically in Fig. 3.

Expression (3) for the energy density has been used in [7] for the numerical simulation of stretching experiments of sheets of nematic elastomer, held between two rigid clamps. A representative volume ele-

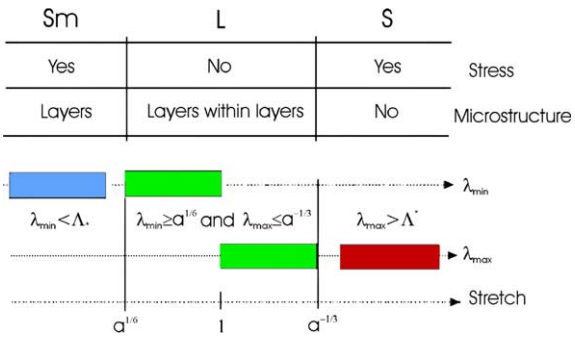

Fig. 3. Schematic summary of the macroscopic response of nematic elastomers. Functions Λ_* and Λ^* are defined in the text.

ment in the center of the sample (i.e., in the left bottom corners of the snapshots in Fig. 5) evolves essentially along the (soft) deformation path of Eq. (4) developing the stripe domain pattern associated to the two deformation gradients (5). Closer to the clamped ends, however, the influence of the clamps is felt more strongly. In fact, the clamps do not allow lateral contraction, hindering substantially the reorientation of the director towards the direction of the imposed stretch. This constraint decays away from the clamped ends producing two interesting effects. On one hand, the induced microstructures are spatially inhomogeneous, with director reorientation occurring more rapidly in the regions far from the clamps. On the other hand, the stress–strain response shows a marked dependence on the geometry of the sample, with the influence of the clamps becoming less pronounced as the aspect ratio length/width increases. These effects are documented in Figs. 4 and 5, which show good qualitative agreements with experimental results from the Cavendish Laboratories [35], and with X-ray scattering measurements in [36].

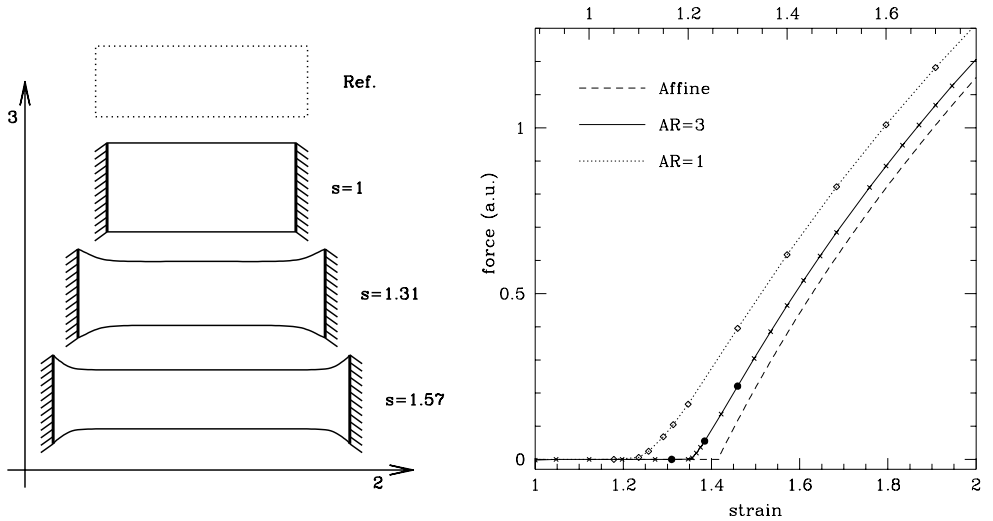

Fig. 4. Numerical simulation of stretching experiments on thin sheets of nematic elastomers: geometry (left) and force–stretch diagrams for several aspect ratios AR (right). The geometry on the left corresponds to AR = 3, which is the case analyzed in detail in the text. On the corresponding force–stretch curve on the right panel, full dots mark the representative points of the configurations shown in Fig. 5 (adapted from [7]).

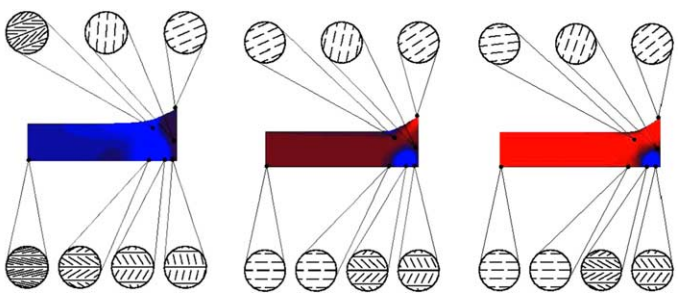

Fig. 5. Numerical simulation of stretching experiments on thin sheets of nematic elastomers, based on the coarse-grained energy W_{qc}, at stretches 1.31, 1.38, 1.46. Only one-quarter of the sample is shown since the rest of the solution can be obtained by symmetry. The circular insets display energetically optimal microstructures at some selected locations within the sample. The sticks in the circular insets hint at the local orientation of the nematic director (adapted from [7]).

3. Ferromagnetic shape memory alloys

Magnetostrictive solids are those in which reversible deformations can be induced by an applied magnetic field. Typical configurations of magnetostrictive bodies under no applied field contain domains on which strain and magnetization are approximately constant. Such domain patterns arise from the interaction of crystallography (because of the existence of preferred crystallographic directions: the easy axes of magnetization) with long range dipolar effects (which, in particular, promote magnetization fields that are tangential to the boundary and hence disfavor configurations with uniform magnetization throughout the specimen). Upon application of a field, there is a redistribution of the domains caused by the fact that certain easy axes are more favorably oriented towards the applied field. Since domains with different magnetization also have different strains, this cooperative redistribution also leads to a macroscopic strain (see, e.g., [10]).

Magnetostriction is typically a small effect. However, giant magnetostrictive materials, developed by Clark and his co-workers in the 1970's, have strains of the order of 10^{-3}. Among these, the alloy $Tb_{0.3}Dy_{0.7}Fe_2$ has enjoyed the greatest commercial success as an actuator material [6]. More recently, a new concept of magnetostriction has emerged, termed ferromagnetic shape memory [20]. Ferromagnetic shape memory materials such as Ni_2MnGa or Fe_3Pd undergo a reversible first order martensitic phase transformation upon cooling, and are also ferromagnetic. The crystallography of twinning implies that neighboring variants have nearly perpendicular easy axes, and therefore, the specimen can be biased toward one variant or another by applying a magnetic field. Because the transformation is first order, unlike in ordinary or giant magnetostrictive materials in which the ferromagnetic transition is second order, very large strains can be produced by variant redistribution, [31,26].

A well-established variational model, called Micromagnetics [3,4], is in principle available to describe the magneto-mechanical response of magnetostrictive solids. This variational model focusses on the microscopic origin of macroscopic deformations, which are ultimately due to distorsions of the crystalline lattice. The general micromagnetic problem for reasonably large samples is, however, difficult because of the necessity of resolving exceedingly complex three-dimensional domain structures.

For this reason it is appealing to try to make use of the special features of some magnetostrictive and ferromagnetic shape memory materials to simplify the general micromagnetic problem. We do this in two ways. First, we make use of the large body limit, as is done in the purely magnetic case in [9]. This is equivalent to neglecting exchange energy and then studying the minimizing sequences of the total energy. Second, we study the limit of high anisotropy. This is done by examining the properties of a minimizing sequence of the energy as the anisotropy constants tend to infinity. This has the effect of imposing a large energetic penalty to a (strain, magnetization) pair that does not lie on the energy wells. For the technical details of the derivation of the simplified model from micromagnetics, we refer to [16]. In the rest of the paper we focus instead on a more informal description of the limit theory, with a view towards its concrete applications to specific problems.

Consider a single crystal occupying the region of space Ω. The state of the material at a point $\mathbf{x}$ in Ω is described by the values at $\mathbf{x}$ of the magnetization vector $\mathbf{M}(\mathbf{x})$ and of the strain tensor $\mathbf{E}(\boldsymbol{x})$. The former field satisfies the condition of local saturation $|\mathbf{M}(\mathbf{x})| = M_s$, where the constant $M_s > 0$ is the saturation magnetization at the (fixed) temperature under consideration. The latter field satisfies the kinematic compatibility condition $2\mathbf{E}_{ij}(\mathbf{x}) = \partial \mathbf{u}_i(\mathbf{x})/\partial x_j + \partial \mathbf{u}_j(\mathbf{x})/\partial x_i$, where $\mathbf{u}(\mathbf{x})$ is the value at $\mathbf{x}$ of the displacement $\mathbf{u}$, a continuous vector field.

Stable equilibria are described as the minima of a free-energy functional

$$E = E_{\mathrm{mel}} + E_{\mathrm{mst}} + E_{\mathrm{ext}}, \tag{9}$$

where the individual summands appearing in (9) are described below. E_{mst} is the magnetostatic energy, i.e., the energy stored in the magnetic field generated by Ω

$$E_{\mathrm{mst}} = -\frac{1}{2}\int_{\Omega} \mathbf{M}(\mathbf{x}) \cdot \mathbf{H}_{\mathbf{M}}(\mathbf{x}) \mathrm{d}\mathbf{x}, \tag{10}$$

where $\mathbf{H}_{\mathbf{M}}$ is the magnetic field induced by $\mathbf{M}$. This is the unique square integrable field that solves Maxwell's equations of magnetostatics, i.e. $\mathrm{curl}\,\mathbf{H}_{\mathbf{M}} = 0$ and $\mathrm{div}\,(\mathbf{H}_{\mathbf{M}} + \mathbf{M}) = 0$ in R^3 (in these equations $\mathbf{M}$ has been extended by zero to R^3). Moreover, E_{ext} is the energy associated with external magnetomechanical loads (here uniform surface tractions at the boundary of Ω, described by a stress tensor $\mathbf{S}$, and a uniform applied magnetic field $\mathbf{H}$):

$$E_{\mathrm{ext}} = -\int_{\Omega} [\mathbf{H} \cdot \mathbf{M}(\mathbf{x}) + \mathbf{S} \cdot \mathbf{E}(\mathbf{x})] \mathrm{d}\mathbf{x}. \tag{11}$$

Finally, E_{mel} is the magnetoelastic energy:

$$E_{\mathrm{mel}} = \int_{\Omega} W(\mathbf{M}(\mathbf{x}), \mathbf{E}(\mathbf{x})) \mathrm{d}\mathbf{x}. \tag{12}$$

In (12), W is the magnetoelastic energy density (elastic plus magneto-crystal-line), a non-negative function whose zeroes describe the pairs of magnetization and deformation which are energetically favored by the anisotropy of the crystalline lattice. The zero level set of the function W, which we call the set $\mathscr{K}$ of the energy wells of the material under consideration

$$\mathscr{K} = \{(\mathbf{M}_1, \mathbf{E}_1), \ldots, (\mathbf{M}_N, \mathbf{E}_N)\}, \tag{13}$$

has a special geometric structure deriving from the material's crystallographic symmetries. This set plays a crucial role in our developments (note that, in particular, $\mathscr{K}$ is a non-convex set and the function W is non-convex).

In writing (9), we have omitted the exchange energy term E_{exch}, which penalizes spatial variations of $\mathbf{E}$ and $\mathbf{M}$ (domain walls). In fact, the simultaneous presence among the energy terms of the non-convex functional E_{mel} and of the magnetostatic energy E_{mst} leads to minimum energy configurations exhibiting fine scale spatial oscillations, which can be interpreted as microscopic domain patterns. The exchange energy E_{exch} is essential in determining the geometry and the length scales of these patterns while, at least in the large body limit, it seems immaterial in determining the macroscopic averages over Ω of the magnetization and of the strain, which are the quantities of interest here. This statement has been proved in [9] for the case in which magnetoelastic interactions are negligible. Although a rigorous proof in the presence of magnetoelastic coupling is not available, indications that this may be still be true come from comparison of computed magnetostriction curves with experimental evidence (see e.g., [10,11]).

The next step in the formulation of our simplified variational model is to restrict the set of admissible configurations to those which only take values on the set of the energy wells $\mathscr{K}$, in order to enforce the high anisotropy limit. In fact, the precise formulation of this constraint, which we may informally express as

$$(\mathbf{M}(\mathbf{x}), \mathbf{E}(\mathbf{x})) \text{ essentially belongs to } \mathscr{K} \text{ almost everywhere in } \Omega, \tag{14}$$

requires considerable care (in fact, it is a constraint on the support of the Young measures generated by energy minimizing sequences, see [16]). The "essentially" in (14) refers to the fact that the constraint can be violated in what we call "transition layers", i.e., the sets of negligible small volume and energy content. In fact our simplified model is asymptotic in nature, and it arises in the limit of inifinitely hard magnetomechanical moduli, as a prototype model for materials governed by energy densities W which grow steeply away from the energy wells $\mathscr{K}$.

With hypothesis (14), the only admissible macroscopic deformations are those obtained by assembling magnetoelastic domains, in which the state variables lie on the material's energy wells. In order that the resulting model be non-trivial, it is necessary that the average deformations compatible with (14) and with

the constraint of kinematic compatibility be larger than the discrete set of uniform deformations contained in $\mathscr{K}$. In this case, configurations mixing magnetization-deformation pairs lying in the energy wells are indeed possible. Their energy, however, may depend in a complex way on fine geometric details, as it would be true, for example, in the case of an interface between two magnetic domains across which the normal component of the magnetization suffers a jump discontinuity. It can be shown that, provided that the energy wells satisfy the following hypothesis of "pairwise magnetoelastic compatibility"

$$2(\mathbf{E}_j - \mathbf{E}_k) = \mathbf{a}_{jk} \otimes \mathbf{n}_{jk} + \mathbf{n}_{jk} \otimes \mathbf{a}_{jk}, \tag{15}$$

$$(\mathbf{M}_j - \mathbf{M}_k) \cdot \mathbf{n}_{jk} = 0, \tag{16}$$

for some pair of vectors $\mathbf{a}_{jk}$ and $\mathbf{n}_{jk}$, with $|\mathbf{n}_{jk}| = 1$ and for every possible choice of the indices $j, k = 1, \ldots, N$, then the set of admissible macroscopic states is given by the convex hull of $\mathscr{K}$, see [16]. Here $\otimes$ denotes the tensor product of two vectors, i.e., $(b \otimes c)_{ij} = b_i c_j$, and no sum on repeated indices is tacitly assumed in (15) or (16).

Conditions (15) and (16) are best explained with reference to a concrete example. Consider the case

$$\mathscr{K} = \{(\pm\mathbf{M}_1, \mathbf{E}_1), (\pm\mathbf{M}_2, \mathbf{E}_2)\}. \tag{17}$$

Pairwise magnetoelastic compatibility is satisfied provided that there exist a unit vector $\mathbf{n}$ and a vector $\mathbf{a}$ such that

$$2(\mathbf{E}_2 - \mathbf{E}_1) = \mathbf{a} \otimes \mathbf{n} + \mathbf{n} \otimes \mathbf{a}, \tag{18}$$

$$(\mathbf{M}_2 - \mathbf{M}_1) \cdot \mathbf{n} = 0. \tag{19}$$

Eq. (18) expresses the condition of kinematic compatibility (6) in the context of linearized kinematics. Arguing as in the previous section, we can use a simple layer construction to approximate any average deformation

$$\langle \mathbf{E} \rangle = \lambda \mathbf{E}_1 + (1 - \lambda)\mathbf{E}_2, \quad 0 < \lambda < 1 \tag{20}$$

by using only the two strains lying in the material's energy wells. Here λ is the volume fraction of the sample where the strain is $\mathbf{E}_1$. In these layers we can let the magnetization be equal to $\mathbf{M}_1$, while setting it equal to $\mathbf{M}_2$ in the complementary layers. In this way, $(\mathbf{M}(\mathbf{x}), \mathbf{E}(\mathbf{x})) \in \mathscr{K}$ (so that the energy W vanishes identically) and the average magnetization is

$$\langle \mathbf{M} \rangle = \lambda \mathbf{M}_1 + (1 - \lambda)\mathbf{M}_2, \quad 0 < \lambda < 1. \tag{21}$$

In addition, condition (19) guarantees that no magnetostatic energy builds up at the layer interfaces, because $\mathbf{M}(\mathbf{x})$ is locally divergence free. therefore, magnetostatic energy is only due to the field $\mathbf{H}_{\langle \mathbf{M} \rangle}$ generated by the macroscopic average $\langle \mathbf{M} \rangle$. We have thus shown that, for every $\langle \mathbf{M} \rangle$ in the convex hull of $\{\mathbf{M}_1, \mathbf{M}_2\}$ and for every $\langle \mathbf{E} \rangle$ in the convex hull of $\{\mathbf{E}_1, \mathbf{E}_2\}$ we can always construct an approximating microstructure $(\mathbf{M}(\mathbf{x}), \mathbf{E}(\mathbf{x}))$ taking only values in the material's energy wells, and whose energy is

$$\frac{1}{2}\langle \mathbf{M} \rangle \cdot \int_\Omega \mathbf{H}_{\langle \mathbf{M} \rangle}(\mathbf{x}) \mathrm{d}\mathbf{x} - |\Omega|(\mathbf{H} \cdot \langle \mathbf{M} \rangle + \mathbf{S} \cdot \langle \mathbf{E} \rangle). \tag{22}$$

By inserting a magnetic substructure alternating $\pm\mathbf{M}_i$ in the layers deformed according to $\mathbf{E}_i$, the same argument applies to any pair of magnetization and deformation in the convex hull of the set (17). The more general sets $\mathscr{K}$ of the form (13) can be handled by iterating the construction above, hence generating complex, sequentially layered microstructures. In these cases, the role of transition layers is essential (see [16] for additional details).

Interestingly, as a consequence of the crystallographic symmetry properties of $\mathscr{K}$, hypotheses (15) and (16) are satisfied in the large majority of the cases of interest for applications. Furthermore, if Ω is an ellip-

soid, the smallest possible energy compatible with configurations with average magnetization $\langle \mathbf{M} \rangle$ and average deformation $\langle \mathbf{E} \rangle$, where

$$\langle \mathbf{M} \rangle = \sum_{i=1}^{N} \lambda_i \mathbf{M}_i, \quad \langle \mathbf{E} \rangle = \sum_{i=1}^{N} \lambda_i \mathbf{E}_i \tag{23}$$

is given by the formula

$$|\Omega| \left(\frac{1}{2} \langle \mathbf{M} \rangle \cdot \mathbf{D} \langle \mathbf{M} \rangle - \mathbf{H} \cdot \langle \mathbf{M} \rangle - \mathbf{S} \cdot \langle \mathbf{E} \rangle \right). \tag{24}$$

The demagnetizing tensor $\mathbf{D}$ appearing in (24) is such that

$$\mathbf{H}_{\langle \mathbf{M} \rangle} = -\mathbf{D} \langle \mathbf{M} \rangle \tag{25}$$

and it depends exclusively on the geometry of the ellipsoid Ω. The scalars λ_i, $i = 1, \ldots, N$, appearing in (23), the ith of which has the physical meaning of the volume fraction of Ω where the state variables have value $(\mathbf{M}_i, \mathbf{E}_i)$, satisfy the relations

$$\sum_{i=1}^{N} \lambda_i = 1; \quad \lambda_i \in [0,1], \quad i = 1, \ldots, N. \tag{26}$$

Computing the average deformation corresponding to minimum energy configurations under the applied magnetic field $\mathbf{H}$ and under the applied surface tractions $\mathbf{S}$ is thus reduced to the problem of minimizing the macroscopic effective energy (24), a quadratic function of the unknown scalars λ_i, subject to the linear constraints (23). This is a quadratic programming problem, which can be easily solved either in closed form, by using the Kuhn–Tucker optimality conditions, or numerically using standard software packages.

Fig. 6 shows a typical set of results that can be obtained by the application of the theory. These include phase diagrams indicating the regions of stability of the various types of microstructures depending on the strength of the applied loads, and computation of magnetization and magnetostriction curves obtained by plotting suitable components of the average fields (23) as functions of the applied magnetic field.

The model described above has been used, e.g., in [30,17] for the prediction of magnetostriction curves for a specimen of Ni_2MnGa under a variety of applied magnetic fields and stresses. Also applications of the

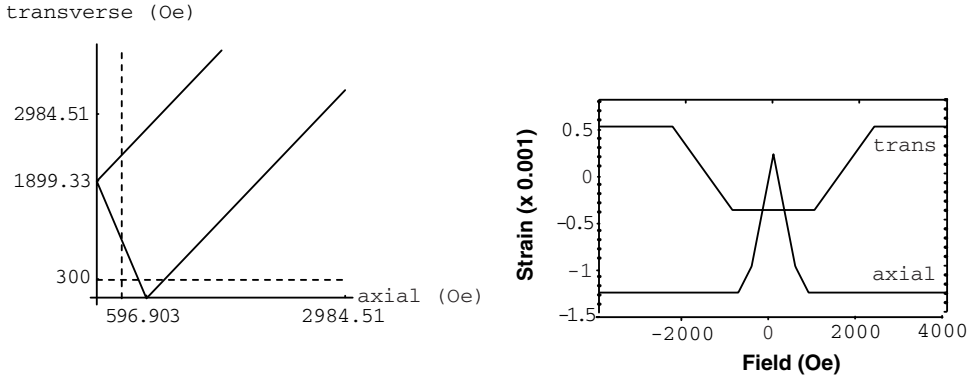

Fig. 6. Numerical simulations for a cylindrical sample of Ni_2MnGa. The left panel shows a phase diagram under combinations of fields applied along the axis or perpendicular to the axis of the sample, and two loading paths (dashed lines). For these two loading paths, the corresponding magnetostriction curves drawn in the right panel. There, the label 'axial' refers to an experiment with fixed transversal and variable axial magnetic field (horizontal loading path), while the label 'trans' refers to the experiment with fixed axial and variable transversal field (vertical loading path).

model to Terfenol-D (which exhibits large conventional magnetostriction, but no field-induced martensitic phase transformation) have been considered [15], leading to the identification of the main domain rearrangement phenomena explaining the experimental observations of [29].

4. Conclusions and outlook

Bridging across length scales is one of the fundamental challenges in the computational modelling of material systems whose mechanical response is driven by rough energy landscapes. Their typical feature is that of exhibiting fine scale microstructures. The two case studies of nematic elastomers and ferromagnetic shape memory alloys discussed in this paper show that hybrid analytical-computational approaches, in which the original problem is first simplified with the use of mathematical analysis, and then attacked computationally, have a great potential in shedding light on systems whose mechanical response is microstructure-driven. In fact, similar strategies are now being applied also to the study of crystal plasticity, following the approach pioneered in [28,5,23].

For the specific systems discussed in this paper, there are several open problems which are worth of consideration. For nematic elastomers, there are, for example, the issues of small but finite compressibility (see [32] for progress on solving some of the related mathematical problems), the issue of anisotropy and semisoftness (see [8] for some progress in this direction), and the impact of finite extensibility of polymer chains (which would lead to a non-neohookean expressions for the microscopic energy density). Regarding the last point, one should emphasize that the regime of small imposed stretches, for which the neohookean expression is a valid approximation, is the most relevant from the point of view of material instabilities and pattern formation. Considering, however, alternative models in which the microscopic energy density has, say, a Mooney–Rivlin-type or an Ogden-type expression (see, e.g., [27]) would be interesting from a mathematical point of view, and it would lead to more realistic stress–strain diagrams in the regime of large imposed stretches.

For ferromagnetic shape memory alloys (and for very closely related systems, such as ferroelectrics), the field is even more open. A less constrained model than the one presented here, in which magnetization rotation is not ruled out by the limit of infinite anisotropy, is certainly desirable. More generally, a detailed understanding of the way in which applied stresses affect twin boundary mobility is one of the most pressing challenges to make sense of experimental observations, while the development of microstructure-based models of hysteresis and of dissipation mechanisms will be crucial in the design of actual devices.

Acknowledgments

It is a pleasure to acknowledge my gratitude towards my coworkers S. Conti, G. Dolzmann, and R.D. James. The results presented in this paper draw from ongoing collaborations with them. In addition, I would like to thank S. Müller for the innumerable enlightening discussions I have had with him in the last five years.

References

[1] J.M. Ball, R.D. James, Fine phase mixtures as minimizers of energy, Arch. Rat. Mech. Anal. 100 (1987) 13–52.
[2] P. Bladon, E.M. Terentjev, M. Warner, Transitions and instabilities in liquid-crystal elastomers, Phys. Rev. E 47 (1993) R3838–R3840.
[3] W.F. Brown, Micromagnetics, J. Wiley Interscience, New York, 1963.
[4] W.F. Brown, Magnetoelastic Interactions, Springer-Verlag, Berlin, 1966.

[5] C. Carstensen, K. Hackl, A. Mielke, Nonconvex potentials and microstructure in finite-strain plasticity, Proc. Roy. Soc. London A 458 (2002) 299–317.
[6] A.E. Clark, High power rare-earth magnetostrictive materials, in: C.A. Rogers, R.C. Rogers (Eds.), Recent Advances in Adaptive and Sensory Materials, Technomic Publishing Inc., 1992.
[7] S. Conti, A. DeSimone, G. Dolzmann, Soft elastic response of stretched sheets of nematic elastomers: a numerical study, J. Mech. Phys. Solids 50 (2002) 1431–1451.
[8] S. Conti, A. DeSimone, G. Dolzmann, Semi-soft elasticity and director reorientation in stretched sheets of nematic elastomers, Phys. Rev. E 60 (2002) 617101–617108.
[9] A. DeSimone, Energy minimizers for large ferromagnetic bodies, Arch. Rat. Mech. Anal. 125 (1993) 99–143.
[10] A. DeSimone, Magnetostrictive solids: macroscopic response and microstructure evolution under applied magnetic fields and loads, J. Intelligent Mat. Syst. Struct. 5 (1994) 787–794.
[11] A. DeSimone, The effect of applied loads on the magnetostrictive response of a Terfenol-D-type material, Scr. Metall. Mater. 33 (1995) 1869–1875.
[12] A. DeSimone, Energetics of fine domain structures, Ferroelectrics 222 (1999) 275–284.
[13] A. DeSimone, G. Dolzmann, Material instabilities in nematic elastomers, Physica D 136 (2000) 175–191.
[14] A. DeSimone, G. Dolzmann, Macroscopic response of nematic elastomers via relaxation of a class of SO(3)-invariant energies, Arch. Rat. Mech. Anal. 161 (2002) 181–204.
[15] A. DeSimone, R.D. James, A theory of magnetostriction oriented towards applications, J. Appl. Phys. 81 (1997) 5706–5708.
[16] A. DeSimone, R.D. James, A constrained theory of magnetoelasticity, J. Mech. Phys. Solids 50 (2002) 283–320.
[17] A. DeSimone, R.D. James, Energetics of magnetoelastic domains in ferromagnetic shape memory alloys, J. Phys. IV France 112 (2003) 969–972.
[18] H. Finkelmann, I. Kundler, E.M. Terentjev, M. Warner, Critical stripe-domain instability of nematic elastomers, J. Phys. II France 7 (1997) 1059–1069.
[19] E. Fried, V. Korchagin, Striping of nematic elastomers, Int. J. Solids Struct. 39 (2002) 3451–3467.
[20] R.D. James, M. Wuttig, Magnetostriction of martensite, Philos. Mag. A 77 (1998) 1273–1299.
[21] J. Küpfer, H. Finkelmann, Nematic liquid single-crystal elastomers, Makromol. Chem. Rapid Commun. 12 (1991) 717–726.
[22] I. Kundler, H. Finkelmann, Strain-induced director reorientation in nematic liquid single crystal elastomers, Macromol. Rapid Commun. 16 (1995) 679–686.
[23] C. Miehe, J. Schotte, M. Lambrecht, Homogenization of inelastic solid materials at finite strains based on incremental minimization principles, J. Mech. Phys. Solids 50 (2002) 2123–2167.
[24] J. Lubliner, F. Auricchio, Generalized plasticity and shape memory alloys, Int. J. Solids Struct. 33 (1996) 991–1003.
[25] S. Müller, Variational models for microstructure and phase transitions, in: F. Bethuel, G. Huisken, S. Müller, K. Steffen, S. Hildebrandt, M. Struwe (Eds.), Calculus of Variations and Geometric Evolution Problems, Lectures given at the 2nd Session of the Centro Internazionale Matematico Estivo, Cetraro 1996, Springer-Verlag, Berlin, 1999.
[26] S.J. Murray, M. Marioni, S.M. Allen, R.C. O'Handley, T.A. Lograsso, 6% magnetic field induced strain by twin-boundary motion in ferromagnetic Ni–Mn–Ga, Appl. Phys. Lett. 77 (2000) 886–888.
[27] R.W. Ogden, Non-Linear Elastic Deformations, Ellis Horwood, Chichester, 1984.
[28] M. Ortiz, E.A. Repetto, Nonconvex energy minimization and dislocation structures in ductile single crystals, J. Mech. Phys. Solids 47 (1999) 397–462.
[29] J.P. Teter, M. Wun-Fogle, A.E. Clark, K. Mahoney, Anisotropic perpendicular axis magnetostriction in twinned TbDyFe, J. Appl. Phys. 67 (1990) 5004–5006.
[30] R. Tickle, R.D. James, T. Shield, M. Wuttig, V.V. Kokorin, Ferromagnetic shape memory in the NiMnGa system, IEEE Trans. Magn. 35 (1999) 4301–4310.
[31] K. Ullakko, J.K. Huang, C. Kantner, R.C. O'Handley, V.V. Kokorin, Large magnetic-field-induced strains in Ni_2MnGa single crystals, Appl. Phys. Lett. 69 (1996) 1966–1968.
[32] Silhavý, M., unpublished manuscript.
[33] G.C. Verwey, M. Warner, E.M. Terentjev, Elastic instability and stripe domains in liquid crystalline elastomers, J. Phys. II France 6 (1996) 1273–1290.
[34] M. Warner, E.M. Terentjev, Nematic elastomers—a new state of matter?, Prog. Polym. Sci. 21 (1996) 853–891.
[35] M. Warner, E.M. Terentjev, Liquid Crystal Elastomers, Oxford University Press, Oxford, 2003.
[36] E.R. Zubarev, S.A. Kuptsov, T.I. Yuranova, R.V. Talroze, H. Finkelmann, Monodomain liquid crystalline networks: reorientation mechanism from uniform to stripe domains, Liquid Cryst. 26 (1999) 1531–1540.